ACS APPLIED MATERIALS & INTERFACES

Research Article

www.acsami.org

Exceptional Performance of $TiNb_2O_7$ Anode in All One-Dimensional Architecture by Electrospinning

Sundaramurthy Jayaraman,[†,‡,§,⊥] Vanchiappan Aravindan,*[,†,⊥] Palaniswamy Suresh Kumar,[‡] Wong Chui Ling,[†] Seeram Ramakrishna,*[,§] and Srinivasan Madhavi*[,†,∥]

[†]Energy Research Institute @ NTU (ERI@N), Nanyang Technological University, Research Techno Plaza, 50 Nanyang Drive, Singapore 637553

[‡]Environmental and Water Technology, Center of Innovation, Ngee Ann Polytechnic, Singapore 599489

[§]Center for Nanofibers and Nanotechnology, Department of Mechanical Engineering, National University of Singapore, Singapore 117576

[∥]School of Materials Science and Engineering, Nanyang Technological University, Singapore 639798

Supporting Information

ABSTRACT: We report the extraordinary performance of an Li-ion battery (full-cell) constructed from one-dimensional nanostructured materials, i.e. nanofibers as cathode, anode, and separator-cum-electrolyte, by scalable electrospinning. Before constructing such a one-dimensional Li-ion battery, electrospun materials are individually characterized to ensure its performance and balancing the mass loading as well. The insertion type anode $TiNb_2O_7$ exhibits the reversible capacity of ~271 mAh g^{-1} at current density of 150 mA g^{-1} with capacity retention of ~82% after 100 cycles. Under the same current density, electrospun $LiMn_2O_4$ cathode delivered the discharge capacity of ~118 mAh g^{-1}. Gelled electrospun polyvinylidene fluoride-*co*-hexafluoropropylene (PVdF-HFP) nanofibers membrane is used as the separator-cum-electrolyte in both half-cell and full-cell assembly which exhibit the liquid like conductivity of ~2.9 mS cm^{-1} at ambient conditions. Full-cell, $LiMn_2O_4$|gelled PVdF-HFP|$TiNb_2O_7$ is constructed by optimized mass loading of cathode with respect to anode and tested between 1.95 and 2.75 V at room temperature. The full-cell delivered the reversible capacity of ~116 mAh g^{-1} at current density of 150 mA g^{-1} with operating potential and energy density of ~2.4 V and ~278 Wh kg^{-1}, respectively. Further, excellent cyclability is noted for such configuration irrespective of the applied current densities.

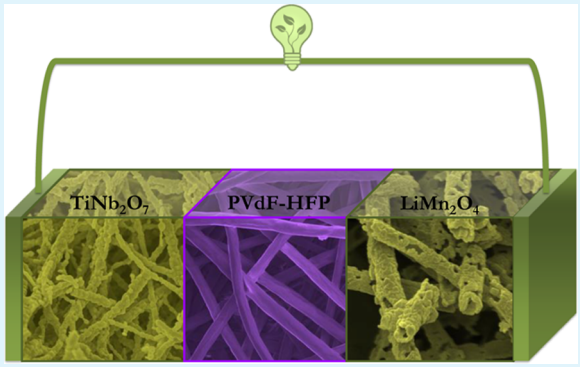

KEYWORDS: *electrospinning, $TiNb_2O_7$, electrospun PVdF-HFP nanofiber membrane, full-cell assembly, Li-ion battery*

INTRODUCTION

One-dimensional nanostructured materials are attractive as prospective electrode and separator-cum-electrolyte for electrochemical energy storage devices particularly lithium-ion batteries (LIBs) by virtue of their high surface to volume ratio, good contact with current collector, and facile Li-diffusion during high current operations.[1,2] There are numerous one-dimensional transition metal oxides and polymer nanostructures, like wires, rods, tubes, fibers, etc., and their derivatives/hybrids with solid or hollow interiors have been reported as electro-active materials for LIB applications.[3−5] Unfortunately, none of the one-dimensional morphologies have been realized for the construction of practical one-dimensional LIBs. In other words, anode/cathode materials have been limited for half-cell configuration or full-cell assembly with commercial bulk powders in the presence of commercial separators.[6] In this regard, we made an novel attempt to utilize the advantages of such one-dimensional nanostructures for the fabrication of the first ever made one-dimensional LIB using fibers.[6] A well established electrospinning technique has been effectively utilized to synthesize one-dimensional nanofibers because of its simplicity and scalability.[7] Cubic spinel $LiMn_2O_4$, monoclininc $TiNb_2O_7$, and polyvinylidene fluoride-*co*-hexafluoropropylene (PVdF-HFP) nanofibers have been chosen for the present study as cathode, anode, and separator-cum-electrolyte, respectively. Spinel phase $LiMn_2O_4$ is a ~4 V vs Li low cost cathode active material with ecofriendliness and an easy synthesis protocol which makes if a preferred candidate for the fabrication of one-dimensional LIBs.[5,8] In addition to above salient features, recently we reported the extraordinary electrochemical performance such nanofibers in half-cell assembly with a Whatman separator.[9] Indeed the compatibility of such an electrode with an ionically conducting electrospun membrane is worth investigating in either half-cell or full-cell

Received: March 12, 2014
Accepted: April 25, 2014
Published: April 25, 2014

Scheme 1. Schematic Representation of Typical Li-Ion Battery Comprising a One-Dimensional Component

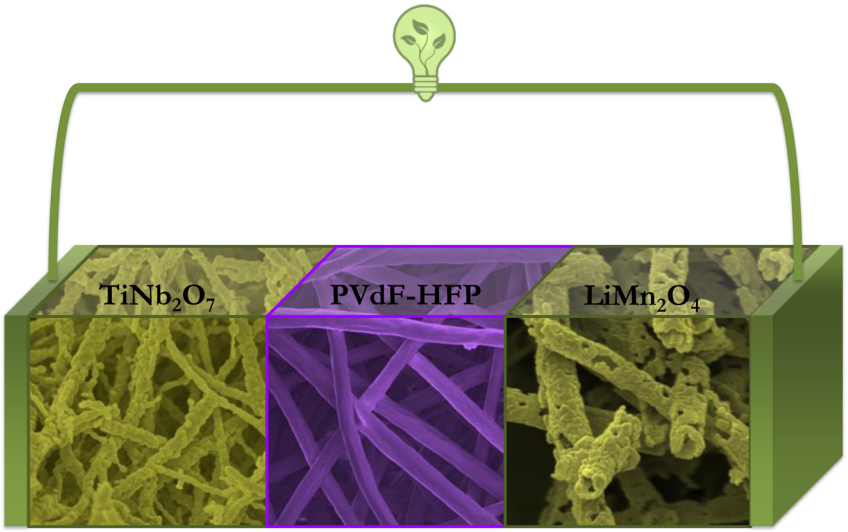

configuration. For the case of insertion type anode, Ti and Nb based framework materials are found beneficial in terms of lower operating potential and ease of synthesis, since the $Ti^{4+/3+}$, $Nb^{5+/4+}$, and $Nb^{4+/3+}$ redox couples generally occur between 1.0 and 1.75 V vs Li which is well matched with the LUMO of conventional carbonate based organic electrolytes ($LiPF_6$ in EC:DMC or EC:DEC).[10,11] Further, $TiNb_2O_7$ exhibits the highest theoretical capacity of insertion type material (388 mAh g^{-1} for a five electron reaction) investigated so far including a graphitic anode with operating potential of ~1.59 V vs Li which is very close to that of zero strain insertion host $Li_4Ti_5O_{12}$ (1.55 V vs Li).[11,12] In this line, Li-insertion properties of electrospun monoclinic $TiNb_2O_7$ nanofibers have been evaluated in half-cell configuration and subsequently employed as the anode in a full-cell assembly in the presence of an electrospun PVdF-HFP nanofiber membrane as separator-cum-electrolyte. It is well-known that PVdF-HFP exhibits very high anodic stability due to the presence of strong electron with drawing (−C−F) functional groups and high dielectric constant (ε = 8.4) which favors the greater dissociation of lithium salts; thus, it provides more number of charge carriers that facilitate enhanced electrochemical performance. Apart from the electrolyte point of view, crystalline VdF and amorphous HFP strands supply the excellent chemistry and plasticity for PVdF-HFP nanofibers, respectively. In addition, electrospun membranes certainly overcome the disadvantages of a conversional liquid electrolyte, particularly the leakage issue, and subsequently provide shape versatility for the construction of various flexible dimensions.[13,14] Further, a multiphase liquid entrapping system of such nanofibers provides the liquid like conductivity and necessary mechanical stability to be used as a separator-cum-electrolyte.[13,15] Due to the fascinating advantages of aforementioned electrodes and separator-cum-electrolyte, we have successfully synthesized one-dimensional nanofibers by electrospinning and subsequently evaluated them in half-cell configuration with the same current density. On the basis of the electrochemical performance of such electrodes in a half-cell configuration, the mass loading has been optimized during the fabrication of a full-cell assembly ($LiMn_2O_4$|PVdF-HFP|$TiNb_2O_7$) and described in detail (Scheme 1).

EXPERIMENTAL SECTION

Electrospun PVdF-HFP Nanofiber Membranes. These were prepared using high molecular weight PVdF-HFP (Kynar Flex 2801, M_w = 4.77 × 10^5, VdF/HFP ratio: 88/12, Elf Atochem). An appropriate amount of PVdF-HFP was dissolved in mixed solvents of acetone/dimethylacetamide with a 7:3 ratio by weight and stirred continuously for 24 h at room temperature. Then, the resulting viscous solution was degassed for 15 min to get a bubble free clear solution which was subsequently fed to the stainless steel needle using a syringe infusion/withdrawal pump (KD Scientific, Model-210). The tip of the needle from the syringe and the Al-foil collector were connected with a high voltage power source. An applied voltage of 20 kV, distance of 20 cm from collector to tip of the spinneret, needle bore size of 0.6 mm, flow rate of 0.2 mL·min^{-1}, and collector drum rotation speed of 150 rpm were optimized to obtain bead free homogeneous ultralong nanofibers. As-spun PVdF-HFP nanofibers were collected over Al-foil as a free-standing nonwoven membrane with thickness of ~150 μm. Then, it was vacuum-dried at 60 °C for 12 h to remove any traces of solvent molecules before conducting electrochemical studies.

One-Dimensional Electrospun $TiNb_2O_7$ and $LiMn_2O_4$ Nanofibers. These were synthesized by a simple electrospinning technique. In the typical synthesis procedure, titanium(IV) butoxide, niobium(V) ethoxide, manganese acetate dihydrate [$Mn(CH_3COO)_2{\cdot}2H_2O$], lithium nitrate and ethanol (HPLC grade), polyvinylpyrolidone (PVP, M_w 130 000), and acetic acid (99.7%) were purchased from Aldrich and used without any further purification.

In a typical synthesis, sol−gel homogeneous solution was prepared by mixing 1.2 g of PVP in 12 mL ethanol under constant stirring for an hour. Then, 0.6 mL titanium(IV) butoxide was added and stirred for an hour, followed by addition of 0.9 mL niobium(V) ethoxide and stirring again to obtain homogeneous polymer solution. Finally, 1 mL of acetic acid was added to the solution under vigorous stirring for ~12 h. The prepared sol−gel solution was then transferred into a 5 mL syringe (diameter of 11.9 mm) with an 18 G stainless steel needle which has a diameter of 0.084 cm. The experiment has been carried out in a controlled electrospinning setup (Electrospunra, Mikrotools Pvt. limited, Singapore). The humidity level of the synthesis electrospinning chamber was maintained at about 35% for the whole experimental process. The distance between needle and static collector (aluminum foil) was maintained at 18 cm with an applied ac voltage of 15 kV and at a flow rate of 1 mL h^{-1}. Finally, the prepared composite fibers were collected and immediately preheated at 300 °C for 1 h and further sintered at 1000 °C, with a heating rate of 5 °C min^{-1} for 4 h under air atmosphere to yield $TiNb_2O_7$ nanofibers.

For synthesis of $LiMn_2O_4$ nanofibers, sol−gel homogeneous solution was prepared by mixing 1.5 g of PVP in 15 mL ethanol

dx.doi.org/10.1021/am501464d | ACS Appl. Mater. Interfaces 2014, 6, 8660−8666

under constant stirring for 1 h. Then, 0.3 g of lithium nitrate and 2.33 g of manganese acetate dehydrate were added simultaneously in the homogeneous polymer solution and stirred again. Finally, 1 mL of acetic acid was added to the solution under vigorous stirring for ~12 h. The prepared sol−gel solution was then transferred into a 5 mL syringe (diameter of 11.9 mm) with an 18 G stainless steel needle which has a diameter of 0.084 cm. The experiment has been carried out in a controlled electrospinning setup (Electrospunra, Mikrotools Pvt. limited, and Singapore). The humidity level of the synthesis electrospinning chamber was maintained at about 35% for the whole experimental process. The distance between the needle and static collector (aluminum foil) was maintained at 16 cm with an applied ac voltage of 22 kV at a flow rate of 0.7 mL h^{-1}. Finally, the prepared composite fibers were collected and immediately preheated at 500 °C for 1 h and further sintered at 800 °C, with a heating rate of 5 °C·min^{-1} for 5 h under air atmosphere (Supporting Information Figure S1).

Powder X-ray diffraction measurements were performed to study the structural properties of electrospun $TiNb_2O_7$ and $LiMn_2O_4$ nanofibers by X-ray diffraction (XRD) measurements using Bruker AXS D8 Advance instrument equipped with Cu Kα radiation. Rietveld refinement was also carried out using Topas V3 software. Morphological features of electrospun anode, cathode, and separator-cum-electrolyte were analyzed by field emission scanning electron microscope (FE-SEM, JEOL JSM-7600F) and transmission electron microscopy (TEM, JEOL 2100F). All the electrochemical studies were performed in standard two electrode coin-cell configuration (CR 2016) at ambient temperature conditions. The composite electrodes were fabricated with accurately weighed active mass loading of 10 mg ($LiMn_2O_4$ or $TiNb_2O_7$ nanofibers), 1.5 mg of Super P, and 1.5 mg of teflonized acetylene black (TAB-2) for half-cell studies. Then the mixture was pressed over a 200 mm^2 area stainless steel mesh (0.25 mm thickness, Goodfellow, UK) current collector. For the half-cell configuration, metallic lithium (Kyokuto Metal Co., Japan; 0.59 mm thick) served as the counter and reference electrode. In both half- and full-cell configurations, test electrodes were separated by electrospun PVdF-HFP membranes gelled with 1 M $LiPF_6$ in ethylene carbonate (EC)/dimethyl carbonate (DMC) mixture (Selectipure LP30, Merck KGaA, Germany). The gelation was carried out for electrospun PVdF-HFP membrane nanofibers by immersion for 5 min in the above solution. For the case of full-cell assembly, anode to cathode mass ratio has been balanced based on the electrochemical performance in half-cell configurations under the same current density. Ionic conductivity measurements of the electrospun PVdF-HFP membranes were studied between −20 and 70 °C using two stainless steel (SS) blocking electrodes (SS|gelled electrospun PVdF-HFP membrane|SS). Electrochemical characterizations were carried out using Solartron 1470E and SI 1255B impedance/gain-phase analyzer coupled with a potentiostat at an ac amplitude of 20 mV over the frequency range of 1 MHz to 10 mHz. Cyclic voltammetry (CV) studies were conducted at slow scan rate of 0.1 mV·s^{-1} in two-electrode configuration, in which metallic lithium acts as both counter and reference electrode. Galvanostatic cycling studies were conducted in ambient temperature conditions using an Arbin battery tester with various current densities.

RESULTS AND DISCUSSION

Electrospinning is the convenient scalable technique to produce the electrospun polymer membranes with continuous fiberous morphology. For the past one decade, electrochemical properties of such fiberous membranes prepared from various polymers have been extensively investigated for LIB applications.[6,14] Figure 1a represents the morphological features of the electrospun PVdF-HFP nanofiber membranes and clearly showed the presence of highly interconnected continuous ultralong bead free fiberous morphology. This showed the rapid evaporation of solvent during electrospinning process and formation of dry fibers on the collection target. The presence of such morphology certainly offers the multiphase system during

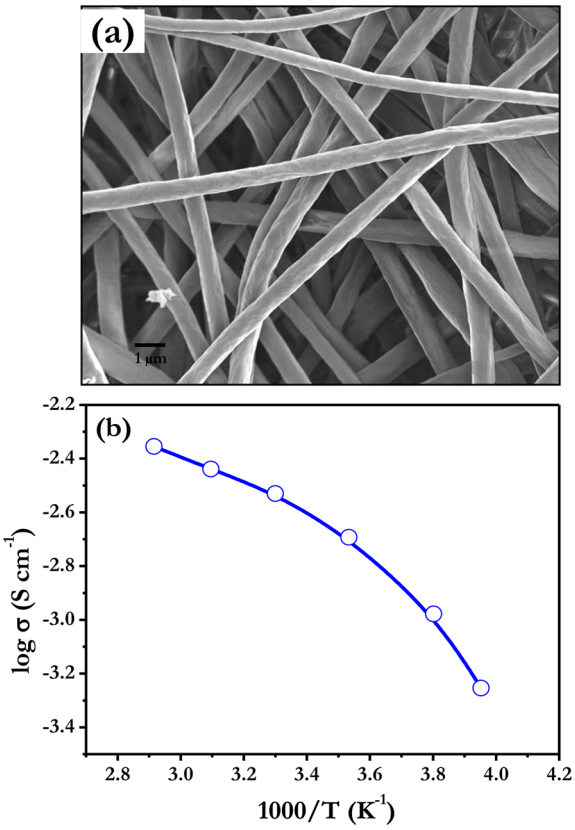

Figure 1. (a) FE-SEM picture of as spun PVdF-HFP nanofiber membrane. (b) Temperature dependent ionic conductivity of electrospun PVdF-HFP nanofibers membrane recorded between two stainless steel blocking electrodes by applying ac amplitude.

gelation process, i.e., swollen gel, crystalline strands, and liquid phase, which is beneficial for the wide temperature operation of the LIB apart from shape versatility.[13,16] Such a multiphase system indeed facilitates faster ionic transport, liquid like conductivity, and lower bulk impedance which provide high rate capability of the cell and render the system as a suitable candidate for high power lithium-ion power packs.[13] However, utilization of such electrospun membranes in practical LIB is very rarely studied (except half-cell configurations).[6,14,17,18] In this line, to realize the performance of one-dimensional nanostructures in practical LIB, an electrospun PVdF-HFP nanofiber membrane was fabricated and subsequently employed as separator-cum-electrolyte. Before conducting the cell assembly, to evaluate the ionic conductivity of such electrospun PVdF-HFP membranes is very crucial. Therefore, temperature dependent ionic conductivity of PVdF-HFP membranes was evaluated between −20 to 70 °C by ac impedance spectroscopy and given in Figure 1b. Ionic conductivity of ~2.9 mS cm^{-1} is noted at 30 °C. Evident from Figure 1b, linear increase in conductivity with temperature is noted which is mainly due to the increase in number of charge carriers because of higher activation energy (E_a) while increasing temperature.[19] In addition, increase in temperature also enables the flexibility and segmental motion of polymer chains. The E_a for ionic conduction can be obtained using the Vogel−Tamman−Fulcher (VTF) model $\sigma = \sigma_0 T^{-1/2} \exp[(-E_a/R(T - T_0)]$ instead of the simple Arrhenius model ($\sigma = \sigma_0 \exp(-E_a/RT)$ used for linear plots. This clearly suggests the conduction mechanism in electrospun nanofibers not only involves the

dx.doi.org/10.1021/am501464d | ACS Appl. Mater. Interfaces 2014, 6, 8660−8666

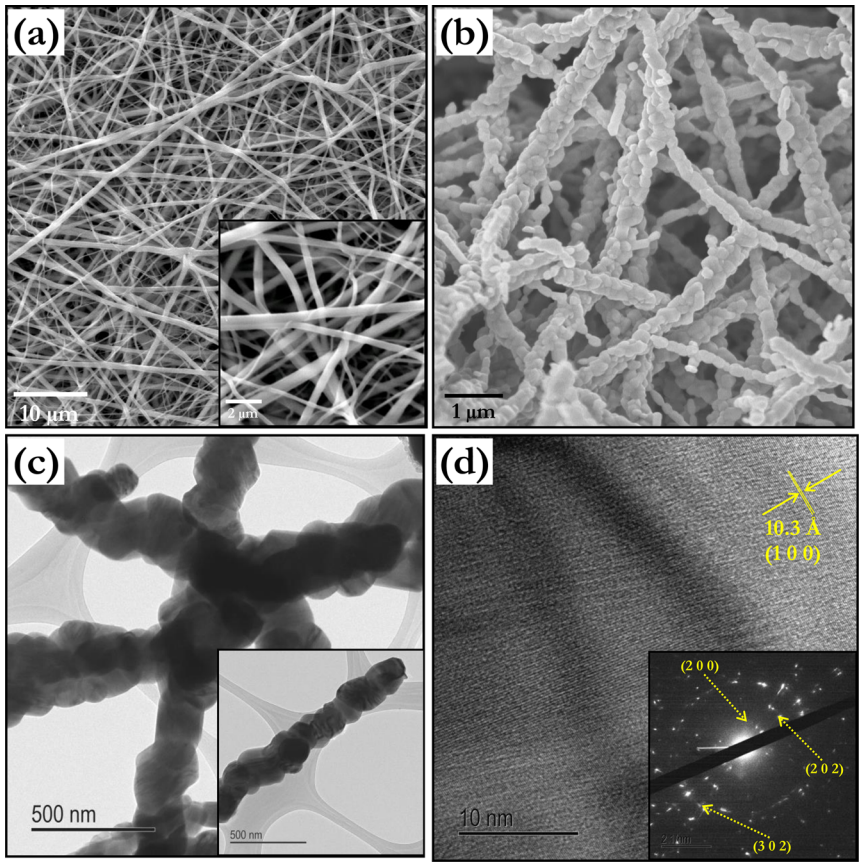

Figure 2. (a) FE-SEM picture of as spun composite $TiNb_2O_7$ nanofibers. (inset) Higher magnification. (b) FE-SEM images of electrospun $TiNb_2O_7$ nanofibers calcined at 1000 °C for 4 h at air atmosphere. (c) TEM picture of calcined $TiNb_2O_7$ nanofibers. (inset) Single nanofiber. (d) HR-TEM pictures showed the orientation of $TiNb_2O_7$ crystals toward the (100) plane. (inset) SAED pattern with corresponding Miller indices.

increasing dissociation of lithium salt and lowering of ionic coupling but also the segmental motion of the polymer chains as well.[10,19]

Morphological features of the electrospun monoclinic $TiNb_2O_7$ nanofibers are illustrated in Figure 2. Highly interconnected network of fibers are noted for as-spun and calcined electrospun nanofibers (Figure 2a and b). A slight reduction in the fiber diameter is observed after the calcination at 1000 °C in air atmosphere, which is presumably due to the decomposition of polymer backbone. The thickness/fiber diameter is ranging from 100 to 300 nm after calcination. The heat treatment at 1000 °C certainly provides the formation of irregularly shaped particulates along with the fiber direction. As a result, formation of one-dimensional nanofibers which comprise attachment of polycrystalline nanosized $TiNb_2O_7$ particulates (Figure 2c and d) occurs. Moreover, such a morphology and particulate formation is common for the case of metal oxide nanofibers prepared by the electrospinning technique which includes spinel phase $LiMn_2O_4$ nanofiber cathodes.[9,20,21]

Figure 3a shows the Rietveld refined XRD pattern of electrospun $TiNb_2O_7$ calcined at 1000 °C for 4 h. The refinement clearly suggests the formation of a single phase material without any impurity traces. The refinement has been carried out based on the assumption of monoclininc structure with $C2/m$ space group. Lattice parameters values are calculated during refinement and found to be a = 11.9171 (6) Å, b = 3.8039 (2) Å, c = 20.3908 (4) Å, and β= 120.313 (8)° which is consistent with the previous report by Wadsley.[22]

The average crystallite size value of ∼57 nm is calculated by the Scherrer equation during refinement. The distorted arrangement of Nb and Ti atoms possesses two-dimensional interstitial spaces for the accommodation of Li during electrochemical charge−discharge process. Cyclic voltammetry (CV) traces of electrospun $TiNb_2O_7$ nanofibers in half-cell configuration was recorded between 1 and 3 V vs Li at slow scan rate of 0.1 mV s^{-1} and presented in Figure 3b. The CV curve showed sharp peaks at ∼1.56 and ∼1.68 V vs Li during the first cathodic and anodic sweeps, respectively. The sharp peak potential during first cathodic sweep at ∼1.56 V vs Li is corresponds to the $Ti^{4+/3+}$ redox couple.[23−25] The presence of downward peak at ∼1.77 V vs Li is associated with $Nb^{5+/4+}$ couple. The appearance of a shoulderlike peak at ∼1.25 V vs Li is ascribed to the $Nb^{4+/3+}$ couple.[23,25] In the subsequent cycles, the prominent cathodic peak shifts slightly toward higher potential (∼1.6 V vs Li) because of the structural rearrangement of host matrix/formatting cycle during first Li-insertion, and it is common for Ti-based insertion type materials.[18,26−28] The constructive and overlapping of CV curves during successive cycles indicates the excellent reversibility of the system. Figure 3c represents the typical galvanostatic charge−discharge curves recorded at constant current density of 150 mA g^{-1} between 1 and 3 V vs Li. The observed cycling curves are consistent with previous work by other researchers.[11,23−25,29] The half-cell delivered discharge capacity of ∼271 mAh g^{-1} with coloumbic efficiency of over 99.5%. The observed reversibility and efficiency is one of the best values reported so far compared to the previous reports on $TiNb_2O_7$; for example, Lu et al.[23]

dx.doi.org/10.1021/am501464d | ACS Appl. Mater. Interfaces 2014, 6, 8660−8666

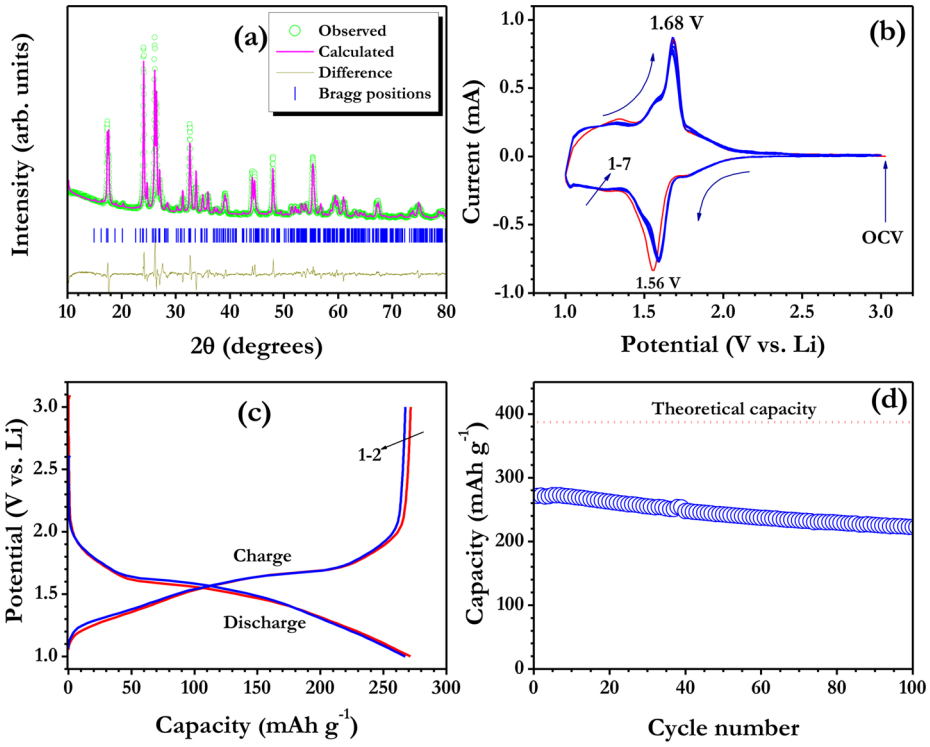

Figure 3. (a) Powder X-ray diffraction pattern of electrospun $TiNb_2O_7$ nanofibers calcined at 1000 °C. (b) CV traces of electrospun $TiNb_2O_7$ nanofibers in half-cell assembly recorded between 1 and 3 V vs Li at scan rate of 0.1 mV s^{-1}, in which metallic lithium acts as both counter and reference electrode. (c) Typical galvanostatic charge−discharge curves at current density of 150 mA g^{-1} and (d) plot of discharge capacity vs cycle number recorded in ambient conditions.

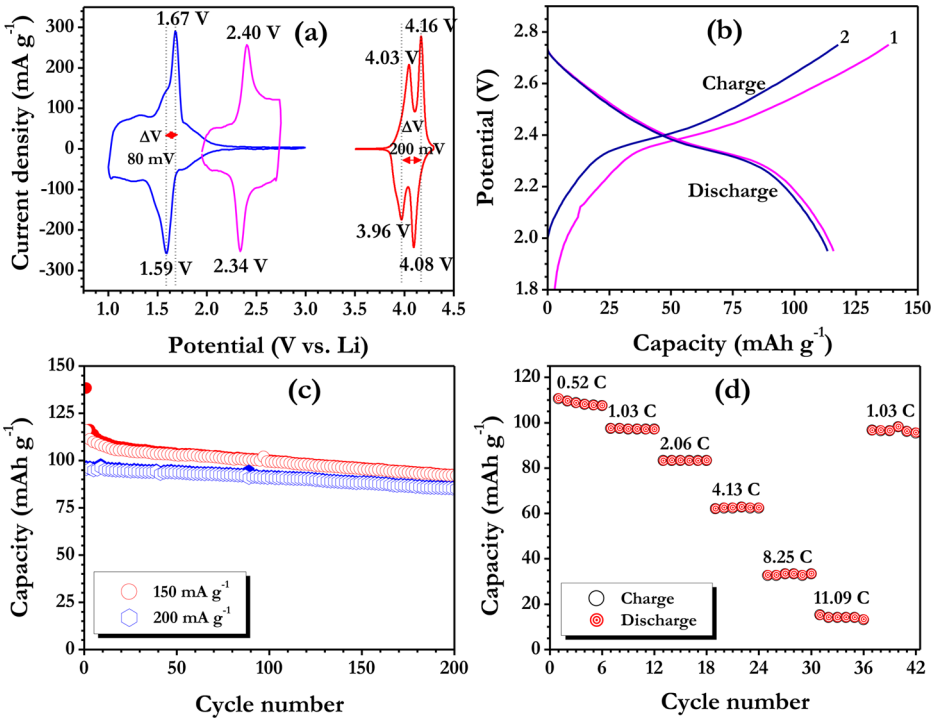

Figure 4. (a) CV traces of all one-dimensional full-cell, $LiMn_2O_4$|gelled PVdF-HFP|$TiNb_2O_7$ tested between 1.95 and 2.75 V at scan rate of 0.1 mV s^{-1}. The electrochemical performance of $TiNb_2O_7$ and $LiMn_2O_4$ electrodes in half-cell assembly is also given for the comparison. (b) Typical galvanostatic charge−discharge curves of full-cell, $LiMn_2O_4$|gelled PVdF-HFP|$TiNb_2O_7$ at current density of 150 mA g^{-1}. (c) Plot of discharge capacity vs cycle number for all one-dimensional full-cell, $LiMn_2O_4$|gelled PVdF-HFP|$TiNb_2O_7$ at current density of 150 and 200 mA g^{-1}. (d) Rate capability studies of all one-dimensional full-cell, $LiMn_2O_4$|gelled PVdF-HFP|$TiNb_2O_7$ cycled between 1.7 and 2.5 V at various C rates (1 C is assumed as 150 mAh g^{-1}).

dx.doi.org/10.1021/am501464d | ACS Appl. Mater. Interfaces 2014, 6, 8660−8666

reported the Li-insertion behavior $TiNb_2O_7$ by solid-state approach and delivered the reversible capacity of ~261 mAh g^{-1} with 93% efficiency at 30 mA g^{-1} current density. Solid-state synthesized $TiNb_2O_7$ delivered reversible capacity of ~233 mAh g^{-1} with 76% efficiency at 0.2 C rate by Saritha and Varadaraju.[25] Carbon-coated $TiNb_2O_7$ showed the initial discharge capacity of ~277 mAh g^{-1} at 0.1 C rate with columbic efficiency of 105%, i.e., the reversible capacity is higher than the insertion capacity between 1 and 2.5 V vs Li by Han et al.[11,29] Further, a slight shift in the Li-insertion potential is noted for the second cycle compared to first cycle which is in good agreement with CV studies. A plot of reversible capacity vs cycle number at current density of 150 mA g^{-1} is illustrated in Figure 3d. The electrospun $TiNb_2O_7$ nanofibers showed good cyclability during cycling; however, capacity fading is noted and retained ~82% of initial reversible capacity after 100 cycles. In the full-cell configuration, cathode $LiMn_2O_4$ is the only source for Li-ions whereas in half-cell assembly metallic Li acts as a reservoir for Li-ions. Therefore, mass balance is necessary and crucial for the complete utilization electro-active material during electrochemical cycling. Based on the performance of both $TiNb_2O_7$ and $LiMn_2O_4$ (Supporting Information Figure S2) in half-cell configuration under same current rate (150 mA g^{-1}), the full-cell is fabricated by adjusting the anode to cathode fixed mass ratio of 1:2.3. Further, in order to avoid the cathode limit, we included excess (5 wt %) of $LiMn_2O_4$ than estimated loading in the full-cell assembly.

Figure 4 represents the electrochemical profiles of all one-dimensional full-cell ($LiMn_2O_4$|PVdF-HFP|$TiNb_2O_7$) assembly tested between 1.95 and 2.75 V in ambient temperature conditions. The full-cell is first charged to extract the Li from the spinel lattice and subsequently inserted in to anode for charge balance. From the CV traces of full-cell clearly showed the predominant redox peaks at ~2.40 and ~2.34 V during anodic and cathodic sweeps, respectively. The occurrence of anodic peak is due to the oxidation of Mn^{3+} to Mn^{4+} in cathode and simultaneous reduction of Ti^{4+} to Ti^{3+} and Nb^{5+} in to Nb^{3+} occurred at $TiNb_2O_7$ lattice and the above redox reaction is reversed during subsequent cathodic scan. Monotonous charge−discharge curves are observed for full-cell configuration with operating potential of ~2.4 V at current rate of 1 C. The theoretical capacity of cathode (148 mAh g^{-1}) is assumed as 1 C, i.e., current density of 150 mA g^{-1}. The cell delivered the capacity of ~138 and ~116 mAh g^{-1} at 1 C rate for first charge and discharge, respectively (calculated based on the cathode active mass). Columbic efficiency of the full-cell is drastically enhanced from ~84 to ~96% from first to second cycle. Further increase in columbic efficiency toward higher percentage is noted during subsequent cycling (Figure 4c). This enhanced columbic efficiency is mainly due to the utilization of one-dimensional electrospun nanofibers which enables facile transportation and diffusion of Li-ions during cycling. Moreover, appropriate mass loading of the electrodes cannot be excluded for such superior performance. Evident from Figure 4c, all one-dimensional full-cell, $LiMn_2O_4$|PVdF-HFP|$TiNb_2O_7$ delivered an extraordinary cyclability irrespective of the applied current densities. After 200 cycles, full-cell retained ~79 and ~89% of initial reversible capacity for current density of 150 and 200 mA g^{-1}, respectively. This performance clearly showed increase in current rate renders good cyclability during prolonged cycling. According to Han et al.,[11,29] poor columbic efficiency and cyclability is noted for carbon-coated $TiNb_2O_7$ anodes when coupled with Ni-doped spinel phase cathode ($LiNi_{0.5}Mn_{1.5}O_4$). This setback has been successfully alleviated by employing one-dimensional electrospun electrodes and separator-cum-electrolyte without any surface modifications. However, the meager capacity fade is noted for both half- and full-cell assembly during cycling, which is due to the intrinsic nature of the insertion type anode $TiNb_2O_7$ (since electrospun $LiMn_2O_4$ cathode displayed an extraordinary cyclability in half-cell configuration, Supporting Information Figure S2). In addition to above, rate performance is one of the important criterions to employ them in high power applications especially electric vehicles.[30] Rate capability studies vindicate the excellent performance of such full-cell irrespective of the C rate during cycling and good capacity retention is also evidenced from Figure 4d. At current density of 150 mA g^{-1}, the full-cell delivered energy density of ~280 Wh kg^{-1} which is comparable to the other commercially available Li-ion configurations.[3,4] Moreover, the energy density can be increased by choosing high potential cathodes preferably ordered spinel phase $LiNi_{0.5}Mn_{1.5}O_4$.[31] The present study clearly demonstrates that, utilization of one-dimensional nanostructures certainly paved the way for the development of high performance Li-ion power packs. Further studies on progress to increase the energy density (i.e., operating potential as well) and suppress the minimal capacity fade by adopting various procedures.

CONCLUSION

To conclude, all one-dimensional Li-ion battery was successfully fabricated and demonstrated with extraordinary performance. All the one-dimensional electro-active materials were prepared by scalable electrospinning and treated with desired conditions. Full-cell was capable of delivering very high reversible capacity of ~116 mAh g^{-1} and the observed values were very close to that of electrospun cathode ($LiMn_2O_4$) under the similar test conditions in half-cell configurations (~118 mAh g^{-1}). Further, full-cell $LiMn_2O_4$|PVdF-HFP|$TiNb_2O_7$ exhibits the working potential and energy density of ~2.4 V and ~280 Wh kg^{-1}, respectively at 1 C rate. The present study clearly proved that the electrospinning technique can certainly provide the new platform to realize the advantages of one-dimensional nanostructured materials in practical Li-ion cells.

ASSOCIATED CONTENT

Supporting Information

Morphological, structural, and electrochemical properties of electrospun $LiMn_2O_2$ nanofibers are given. This material is available free of charge via the Internet at http://pubs.acs.org.

AUTHOR INFORMATION

Corresponding Authors

*E-mail: aravind_van@yahoo.com (V.A.).
*E-mail: seeram@nus.edu.sg (S.R.).
*E-mail: Madhavi@ntu.edu.sg (S.M.).

Author Contributions

⊥S.J. and V.A contributed equally.

Notes

The authors declare no competing financial interest.

■ ACKNOWLEDGMENTS

Authors thank the National Research Foundation (NRF, Singapore) for financial support through the Competitive Research Programme (CRP, Grant no. NRF-CRP4-2008-03)

■ REFERENCES

(1) Manthiram, A. Materials Challenges and Opportunities of Lithium Ion Batteries. *J. Phys. Chem. Lett.* **2011**, *2*, 176−184.
(2) Lee, K. T.; Cho, J. Roles of Nanosize in Lithium Reactive Nanomaterials for Lithium Ion Batteries. *Nano Today* **2011**, *6*, 28−41.
(3) Thackeray, M. M.; Wolverton, C.; Isaacs, E. D. Electrical Energy Storage for Transportation-Approaching the Limits of, and Going Beyond, Lithium-Ion Batteries. *Energy Environ. Sci.* **2012**, *5*, 78547863.
(4) Aravindan, V.; Gnanaraj, J.; Lee, Y.-S.; Madhavi, S. $LiMnPO_4$ - A Next Generation Cathode Material for Lithium-Ion Batteries. *J. Mater. Chem. A* **2013**, *1*, 3518−3539.
(5) Masquelier, C.; Croguennec, L. Polyanionic(Phosphates, Silicates, Sulfates) Frameworks as Electrode Materials for Rechargeable Li(or Na) Batteries. *Chem. Rev.* **2013**, *113*, 6552−6591.
(6) Cavaliere, S.; Subianto, S.; Savych, I.; Jones, D. J.; Roziere, J. Electrospinning: Designed Architectures for Energy Conversion and Storage Devices. *Energy Environ. Sci.* **2011**, *4*, 4761−4785.
(7) Persano, L.; Camposeo, A.; Tekmen, C.; Pisignano, D. Industrial Upscaling of Electrospinning and Applications of Polymer Nanofibers: A Review. *Macromol. Mater. Eng.* **2013**, *298*, 504−520.
(8) Whittingham, M. S. Lithium Batteries and Cathode Materials. *Chem. Rev.* **2004**, *104*, 4271−4302.
(9) Jayaraman, S.; Aravindan, V.; Suresh Kumar, P.; Ling, W. C.; Ramakrishna, S.; Madhavi, S. Synthesis of Porous $LiMn_2O_4$ Hollow Nanofibers by Electrospinning with Extraordinary Lithium Storage Properties. *Chem. Commun.* **2013**, *49*, 6677−6679.
(10) Aravindan, V.; Gnanaraj, J.; Madhavi, S.; Liu, H.-K. Lithium-Ion Conducting Electrolyte Salts for Lithium Batteries. *Chem.—Eur. J.* **2011**, *17*, 14326−14346.
(11) Han, J.-T.; Huang, Y.-H.; Goodenough, J. B. New Anode Framework for Rechargeable Lithium Batteries. *Chem. Mater.* **2011**, *23*, 2027−2029.
(12) Yang, Z.; Choi, D.; Kerisit, S.; Rosso, K. M.; Wang, D.; Zhang, J.; Graff, G.; Liu, J. Nanostructures and Lithium Electrochemical Reactivity of Lithium Titanites and Titanium Oxides: A Review. *J. Power Sources* **2009**, *192*, 588−598.
(13) Choi, S. W.; Jo, S. M.; Lee, W. S.; Kim, Y. R. An Electrospun Poly(vinylidene fluoride) Nanofibrous Membrane and Its Battery Applications. *Adv. Mater.* **2003**, *15*, 2027−2032.
(14) Raghavan, P.; Lim, D.-H.; Ahn, J.-H.; Nah, C.; Sherrington, D. C.; Ryu, H.-S.; Ahn, H.-J. Electrospun Polymer Nanofibers: The Booming Cutting Edge Technology. *React. Funct. Polym.* **2012**, *72*, 915−930.
(15) Aravindan, V.; Sundaramurthy, J.; Kumar, P. S.; Shubha, N.; Ling, W. C.; Ramakrishna, S.; Madhavi, S. A Novel Strategy to Construct High Performance Lithium-Ion Cells Using One Dimensional Electrospun Nanofibers, Electrodes and Separators. *Nanoscale* **2013**, *5*, 10636−10645.
(16) Aravindan, V.; Senthilkumar, V.; Nithiananthi, P.; Vickraman, P. Characterization of Poly(Vinylidenefluoride-co-Hexafluoroprolylene) Membranes Containing Nanoscopic $AlO(OH)_n$ Filler With Li/$LiFePO_4$ Cell. *J. Renewable Sustainable Energy* **2010**, *2*, 033105−6.
(17) Carol, P.; Ramakrishnan, P.; John, B.; Cheruvally, G. Preparation and Characterization of Electrospun Poly (Acrylonitrile) Fibrous Membrane Based Gel Polymer Electrolytes for Lithium-Ion Batteries. *J. Power Sources* **2011**, *196*, 10156−10162.
(18) Aravindan, V.; Shubha, N.; Cheah, Y. L.; Prasanth, R.; Chuiling, W.; Prabhakar, R. R.; Madhavi, S. Extraordinary Long-Term Cycleability of TiO_2-B Nanorods as Anodes in Full-Cell Assembly with Electrospun PVdF-HFP Membranes. *J. Mater. Chem. A* **2013**, *1*, 308−316.
(19) Prasanth, R.; Aravindan, V.; Srinivasan, M. Novel Polymer Electrolyte Based on Cob-Web Electrospun Multi Component Polymer Blend of Polyacrylonitrile/Poly (Methyl Methacrylate)/Polystyrene for Lithium Ion Batteries—Preparation and Electrochemical Characterization. *J. Power Sources* **2012**, *202*, 299−307.
(20) Sahay, R.; Suresh Kumar, P.; Aravindan, V.; Sundaramurthy, J.; Chui Ling, W.; Mhaisalkar, S. G.; Ramakrishna, S.; Madhavi, S. High Aspect Ratio Electrospun CuO Nanofibers as Anode Material for Lithium-Ion Batteries with Superior Cycleability. *J. Phys. Chem. C* **2012**, *116*, 18087−18092.
(21) Aravindan, V.; Suresh Kumar, P.; Sundaramurthy, J.; Ling, W. C.; Ramakrishna, S.; Madhavi, S. Electrospun NiO Nanofibers as High Performance Anode Material for Li-Ion Batteries. *J. Power Sources* **2013**, *227*, 284−290.
(22) Wadsley, A. Mixed Oxides of Titanium and Niobium. I. *Acta Crystallogr.* **1961**, *14*, 660−664.
(23) Lu, X.; Jian, Z.; Fang, Z.; Gu, L.; Hu, Y.-S.; Chen, W.; Wang, Z.; Chen, L. Atomic-Scale Investigation on Lithium Storage Mechanism in $TiNb_2O_7$. *Energy Environ. Sci.* **2011**, *4*, 2638−2644.
(24) Tang, K.; Mu, X.; van Aken, P. A.; Yu, Y.; Maier, J. "Nano-Pearl-String" $TiNb_2O_7$ as Anodes for Rechargeable Lithium Batteries. *Adv. Energy Mater.* **2013**, *3*, 49−53.
(25) Saritha, D.; Varadaraju, U. V. Studies on Electrochemical Lithium Insertion in Isostructural Titanium Niobate and Tantalate Phases with Shear ReO_3 Structure. *Mater. Res. Bull.* **2013**, *48*, 2702−2706.
(26) Aravindan, V.; Chuiling, W.; Madhavi, S. Electrochemical Performance of NASICON Type Carbon Coated $LiTi_2(PO_4)_3$ with a Spinel $LiMn_2O_4$ Cathode. *RSC Adv.* **2012**, *2*, 7534−7539.
(27) Aravindan, V.; Ling, W. C.; Madhavi, S. $LiCrTiO_4$: A High-Performance Insertion Anode for Lithium-Ion Batteries. *ChemPhysChem* **2012**, *13*, 3263−3266.
(28) Zhang, X.; Aravindan, V.; Kumar, P. S.; Liu, H.; Sundaramurthy, J.; Ramakrishna, S.; Madhavi, S. Synthesis of TiO_2 Hollow Nanofibers by Co-Axial Electrospinning and Its Superior Lithium Storage Capability in Full-Cell Assembly with Olivine Phosphate. *Nanoscale* **2013**, *5*, 5973−5980.
(29) Han, J.-T.; Goodenough, J. B. 3-V Full Cell Performance of Anode Framework $TiNb_2O_7$/Spinel $LiNi_{0.5}Mn_{1.5}O_4$. *Chem. Mater.* **2011**, *23*, 3404−3407.
(30) Cairns, E. J.; Albertus, P. Batteries for Electric and Hybrid-Electric Vehicles. *Annu. Rev. Chem. Biomol. Eng.* **2010**, *1*, 299−320.
(31) Julien, C. M.; Mauger, A. Review of 5-V Electrodes for Li-Ion Batteries: Status and Trends. *Ionics* **2013**, *19*, 951−988.